Title

Accelerated ferumoxytol-enhanced 4D multiphase, steady-state imaging with contrast enhancement (MUSIC) cardiovascular MRI: validation in pediatric congenital heart disease

Journal

NMR in Biomedicine, 30(1)

ISSN

0952-3480

Authors

Zhou, Ziwu
Han, Fei
Rapacchi, Stanislas
et al.

Publication Date

2017

DOI

10.1002/nbm.3663

Peer reviewed

HHS Public Access

Author manuscript

NMR Biomed. Author manuscript; available in PMC 2018 January 01.

Published in final edited form as:

NMR Biomed. 2017 January ; 30(1): . doi:10.1002/nbm.3663.

Accelerated Ferumoxytol-Enhanced 4D Multi-phase Steady State Imaging with Contrast Enhancement (MUSIC) Cardiovascular MRI: Validation in Pediatric Congenital Heart Disease

Ziwu Zhou, B.S.[1,2], **Fei Han, Ph.D.**[1,2], **Stanislas Rapacchi, Ph.D.**[1], **Kim-Lien Nguyen, M.D.**[3,4], **Daniel Z Brunengraber, M.D.**[1], **Grace-Hyun J. Kim, Ph.D.**[1], **J. Paul Finn, M.D.**[1,5], and **Peng Hu, Ph.D.**[1,2,5,*]

[1]Department of Radiological Sciences, David Geffen School of Medicine, University of California, Los Angeles, CA, USA

[2]Department of Bioengineering, University of California, Los Angeles, CA, USA

[3]Department of Medicine, Division of Cardiology, David Geffen School of Medicine, University of California, Los Angeles, CA, USA

[4]Division of Cardiology, Veterans Affairs Greater Los Angeles Healthcare System, Los Angeles, CA, USA

[5]Biomedical Physics Inter-Departmental Graduate Program, University of California, Los Angeles, CA, USA

Summary

The purpose of this work was to validate a parallel imaging (PI) and compressed sensing (CS) combined reconstruction method for a recently proposed 4D non-breath-held, multiphase, steady-state imaging technique (MUSIC) cardiovascular MRI in a cohort of pediatric congenital heart disease patients. We implemented a graphics processing unit (GPU) accelerated CS-PI combined reconstruction method and applied it in 13 pediatric patients who underwent cardiovascular MRI after ferumoxytol administration. Conventional breath-held contrast-enhanced MRA (CE-MRA) was first performed during the first-pass of ferumoxytol injection, followed by the original MUSIC and the proposed CS-PI MUSIC during the steady state distribution phase of ferumoxytol. Quality of acquired images were then evaluated using a 4-point scale. Left ventricular volumes and ejection fractions calculated from the original MUSIC and the CS-PI MUSIC were also compared with conventional multi-slice 2D cardiac cine MRI. The proposed CS-PI MUSIC reduced the imaging time of the MUSIC acquisition to 4.6±0.4 min from 8.9±1.2 min. Computationally intensive image reconstruction was completed within 5 min without interruption of sequential clinical scans. The proposed method (mean 3.3–4.0) provided image quality comparable to the original MUSIC (3.2–4.0) (all $P \geq 0.42$), and better than conventional breath-held first-pass CE-MRA (1.1–3.3) for 13 anatomical structures (all $P \leq 0.0014$) with good inter-observer agreement ($\kappa > 0.46$). The calculated ventricular volumes and ejection fractions from both original MUSIC ($r > 0.90$) and the CS-PI MUSIC ($r > 0.85$) correlated well with 2D cine imaging. In conclusion, PI

*Correspondence to: Peng Hu, PhD, Department of Radiological Sciences, 300 UCLA Medical Plaza Suite B119, Los Angeles, CA 90095. penghu@mednet.ucla.edu.

and CS were successfully incorporated into the 4D MUSIC acquisition to further reduce scan time by approximately 50% while maintaining highly comparable image quality in a clinically practical reconstruction time.

Graphical abstract

In this work we implemented and evaluated an accelerated image and fast reconstruction method for a recently proposed 4D multi-phase, steady state imaging technique on a cohort of pediatric patients with congenital heart disease. The image reconstruction was carried out on a custom-built parallelized image reconstruction system that imbedded in the clinical workflow without interrupting normal clinical practice. Proposed strategy reduced the acquisition time of original technique to half and achieved similar image quality and quantitative assessment.

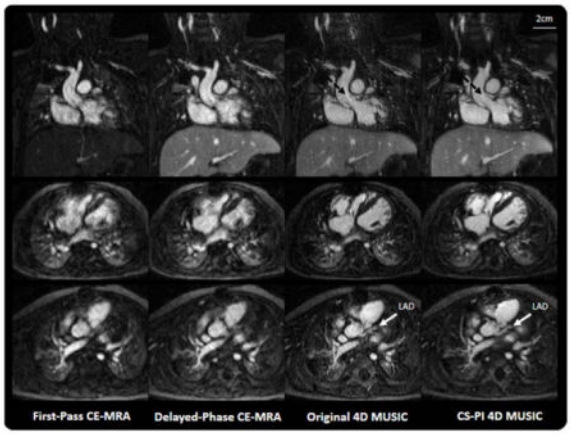

Keywords

ferumoxytol; magnetic resonance angiography; cardiac cine; pediatric MRI; parallel imaging; compressed sensing

Introduction

Contrast-enhanced magnetic resonance angiography (CE-MRA) is increasingly being used to complement echocardiography or replace digital subtraction angiography for anatomic assessment of cardiac and vascular structures in both adults and children (1,2). CE-MRA is typically performed in a breath-hold during the first-pass of a gadolinium-based contrast agent (GBCA) and provides excellent definition of extra-cardiac vascular anatomy (3). Cardiac gating is typically not performed and requires a substantial compromise in resolution due to the time constraints imposed by breath-holding and the need to capture the first-pass of the GBCA. As a result, conventional first-pass CE-MRA provides insufficient definition of pulsatile structures, such as the ventricular outflow tracts, cardiac chambers and coronary arteries. Therefore, supplemental multi-slice 2D cine imaging is required for assessment of cardiac anatomy and volumes. However, 2D cine employs relatively thick slices (3–4 mm), limiting resolution in potentially tiny hearts and precluding useful multi-planar reformatting.

To address these issues, a recent study proposed a 4D multiphase, steady-state imaging (MUSIC) (4) technique in pediatric patients undergoing cardiovascular MRI under general anesthesia and mechanical ventilation. The 4D MUSIC technique acquires multiple cardiac-phase-resolved volumetric images without breath-holding during the steady-state intravascular distribution of ferumoxytol, using the ventilator pressure waveform for respiratory gating. Ferumoxytol, an ultrasmall superparamagnetic iron-oxide (USPIO) particle that is approved by the U.S. FDA for parenteral treatment of iron deficiency anemia in adults with chronic kidney disease, was used off-label to enhance the MUSIC acquisition due to its high R1 relaxivity (r_1 = 9.0 $mM^{-1}s^{-1}$ at 3.0T) and long intra-vascular half-life of 10–14 hours (5). Using 4D MUSIC, a 7–10 minute cardiac- and respiratory-gated scan provides images with improved resolution parameters for both intra- and extra-cardiac anatomy than conventional cardiac magnetic resonance (CMR) techniques such as first-pass CE-MRA or 2D multi-slice cardiac cine imaging (4). In this work, we sought to further accelerate the 4D MUSIC acquisition without compromising image quality.

A variety of fast imaging techniques have been developed for accelerating MR data acquisition. Traditional parallel imaging (PI) methods such as sensitivity encoding (SENSE) (6) and generalized auto-calibrating partially parallel acquisitions (GRAPPA) (7) acquire under-sampled k-space by regularly skipping phase encoding lines. These techniques are widely used clinically due to the reasonable image reconstruction time and their robustness at moderate acceleration factors (3–4X). However, as the acceleration factor increases, poor conditioning of the encoding matrix results in progressively more severe artifacts and noise amplification in the reconstructed image. Recent developments in compressed sensing (CS) (8,9) provide another strategy to accelerate data acquisition (10–12). CS theory states that the image can be recovered from randomly under-sampled k-space data points by using an optimization-based nonlinear reconstruction algorithm with regularization terms incorporated (12–14). With proper choice of regularization terms, the image may be recovered from a higher acceleration factor than using conventional parallel imaging alone. Although long reconstruction times currently limit the widespread clinical use of CS, progress has recently been reported (15, 16) in speeding up certain types of CS image reconstruction algorithms.

In this study, we aimed to take advantage of the high signal-to-noise ratio (SNR) of the ferumoxytol-enhanced 4D MUSIC data by accelerating the MUSIC acquisition with prospective random k-space under-sampling and a joint CS-PI reconstruction technique. The image reconstruction algorithm was implemented in a custom-built parallelized MR image reconstruction system that allowed for clinically acceptable reconstruction time.

Methods

Data Acquisition

The original spoiled gradient recalled echo (GRE)-based 4D MUSIC sequence (4) was modified in such a way that the center 23 × 17 k-space region of the *ky* - *kz* encoding plane was fully sampled while the outer region was under-sampled using a variable-density Poisson-Disk distribution (17), as shown in Figure 1. Each sampled point generated a disk around itself where the probability of a new sample was decreased to ensure maximum

spread of the sampling over the *ky* - *kz* plane. To simulate the variable density sampling, the disk radius was defined as a function of the distance to the center of k-space (*kyc*, *kzc*):

$$Radius_{PDisk}(ky, kz) = 0.3 * \sqrt{(ky - kyc)^2 + (kz - kzc)^2} \quad (1)$$

To mitigate imaging artifacts and signal interference caused by sudden changes in the sampled k-space location, the *ky* - *kz* plane sampling trajectory started from the most central portion of k-space and extended outwards. Samples were sorted and ordered according to their radii and angles to generate a smooth spiral-like, elliptical centric pattern in the *ky* - *kz* plane. This design allowed for sampling of the low frequency data at the beginning of the acquisition, reducing motion sensitivity (18) and eddy-currents effects from high amplitude phase-encoding gradients.

Image Reconstruction

Prospectively under-sampled data were reconstructed separately for each cardiac phase by ℓ_1 -ESPIRiT (19):

$$\hat{d} = \arg\min \sum_{i=1}^{N} \| D\mathcal{F} S_i d - m_i \|_2^2 + \lambda \| W d \|_1 \quad (2)$$

where $\mathcal{F}$ is the Fourier transform; S_i are the sensitivity maps estimated from the center region using ESPIRiT (19); D is the operator that selects the locations where data have been acquired; d is the image to be reconstructed; m_i is the acquired under-sampled k-space data from each of the N receiver coil elements; W is the randomized shifting Daubechies wavelets used to approximate translation invariant wavelets that avoids blocky structural artifacts; and λ is the regularization weight that trades-off between PI data fidelity and the sparsity constraint. In our study, λ was optimized in a pilot study of prospectively under-sampled in vivo data sets acquired on four pediatric congenital heart disease (CHD) patients. We normalized the data sets prior to reconstruction and varied λ from 0.1 to 0.001 in step size of 0.002 to identify the optimal λ value that would provide the best image quality by visual assessment among the reconstructed images. Based on our pilot study, λ was set to 0.004 in our study.

To achieve clinically acceptable reconstruction time, the algorithm was implemented in the C/C++ language based on the Berkeley Advanced Reconstruction Toolbox (20,21) and integrated within a custom-built MR image reconstruction framework (22) in which external computer nodes are connected to the MR scanner directly. K-space data are sent to the nodes for image calculation and reconstructed images are sent back to the scanner system. Figure 2a shows the schematic outline of the framework. Several algorithmic optimizations were incorporated into the reconstruction process to minimize reconstruction time (Figure 2b). First, the coil compression coefficient matrix calculation and 3D coil sensitivity map estimation were performed immediately after the fully-sampled k-space center was acquired, while the sequence continued to acquire the peripheral k-space data. Second, to achieve a

nearly linear reduction of reconstruction time with the number of threads, the non-linear image reconstruction was parallelized across all of the ky - kz slices using the OpenMP framework (23) with eight threads after an initial fast Fourier transform (FFT) was performed in the readout direction.

Phantom Study

In order to evaluate the performance of ℓ_1 -ESPIRiT (19) within our custom-built reconstruction framework, fully-sampled and regularly under-sampled data were acquired using the original 4D MUSIC sequence (4). Prospective randomly under-sampled data were also acquired using the CS-PI 4D MUSIC sequences on a 1.5 Tesla (T) MRI scanner (Magnetom TIM Avanto, Siemens Medical Solutions) with a 12-channel body array coil on a standard American College of Radiology (ACR) MRI phantom. Sequence parameters were: repetition time/echo time (TR/TE) = 2.9/0.9 ms; flip angle, 25°; bandwidth = 814 Hz/pixel; matrix size, 256*256*96; resolution, 1mm isotropic. The fully-sampled data was used as a reference. Three regularly under-sampled data were acquired using three different acceleration schemes: one dimensional acceleration 3X for the in-plane phase-encoding direction and two dimensional accelerations of 2 × 2 and 3 × 2 in both in-plane and through-plane phase-encoding directions. Actual acceleration factors for these three strategies were 2.6X, 3.7X and 5.4X, respectively, due to the fully-sampled center auto-calibration signal. All three regularly under-sampled data were reconstructed with GRAPPA in the vendor-provided reconstruction pipeline. The prospective randomly under-sampled data were acquired in such a way that the acceleration factor was chosen to match the net acceleration factors of the regularly under-sampled acquisitions with consideration of fully sampled center reference lines.

In-vivo Study

Thirteen pediatric CHD patients (aged 4 days to 13 years, six male, heart rate: 95–140 bpm, 118.2± 19.5 bpm) who were referred for clinically indicated cardiovascular MRI independent of our research study were included in our study. Clinical indications included preoperative surgical planning or postoperative evaluation. This HIPAA-compliant study was approved by our institutional review board and written informed consent was obtained from each patient’s legal guardian(s). As our study requires off-label use of ferumoxytol as an MRI contrast agent, we submitted an Investigation New Drug (IND) application (IND # 129441) to the U.S. Food and Drug Administration (FDA) after the FDA boxed regarding ferumoxytol administration in March 2015 and subsequently obtained clearance from the FDA to proceed with our study (NCT02752191). Out of the 13 patients, 1 patient, who was more recently enrolled in our study, underwent imaging under our FDA IND. Each patient either underwent general anesthesia in the MRI suite or was transported directly from the neonatal intensive care unit (NICU) already intubated and sedated. Anesthesia was maintained using a mixture of oxygen and sevoflurane while patients from the NICU were sedated with fentanyl. In all cases, patients were injected with rocuronium bromide as a muscle relaxant. An MR compatible ventilator (Fabius MRI, Drager Medical, Telford, PA) was used with positive end expiratory pressure as clinically appropriate.

All 13 patients were scanned on a 3.0 T MRI scanner (Magnetom TIM Trio, Siemens Medical Solution). Depending on the size of patient, a combination of head coil, flexible coil, body array coil or knee coil was used to provide optimal anatomical coverage. Based on previous studies (4, 24–26), ferumoxytol (Feraheme, AMAG Pharmaceuticals, Lexington, MA) at a dose of 4 mg elemental iron/kg body weight was used in this study. The agent was diluted by 4X-8X and injected at a rate of 0.1–1.0 mL/s. The rate was adjusted so that the bolus duration was approximately 15s, except for one patient who underwent slow infusion of ferumoxytol over 10 min following the recent FDA recommendations in March 2015. To determine the delay time between initiation of the contrast injection and the arrival of the contrast agent in the region of interest, a small bolus of ferumoxytol (0.5 mg/kg) was injected first and the remaining bolus was injected over 15s followed by a chasing saline bolus injected at the same rate. For the patients who underwent bolus injection of ferumoxytol, breath-held CE-MRA was performed under ventilator-controlled breath-holding (VCBH) during the first-pass of ferumoxytol. The same VCBH CE-MRA acquisition was repeated during the steady state distribution phase of ferumoxytol, typically 2–3 min after ferumoxytol injection. Parameters for the first-pass and delayed phase CE-MRA included: TR/TE=2.9/0.9ms; flip angle, 15°; in-plane resolution, 0.9–1.2mm; FOV, 500*300*150 mm; slice thickness, 1.1–1.5mm; GRAPPA acceleration 3X-4X; partial Fourier acquisition (75%) for in-plane and through-plane phase encoding directions; total acquisition time: 18–22s. Subsequently, for all 13 patients, the original 4D MUSIC (4) and the proposed CS-PI 4D MUSIC sequences were performed during the steady state distribution of ferumoxytol without VCBH using the air pressure signal from the ventilator circuit for respiratory gating. The data acceptance window was set to the end-expiration phase and the gating threshold was set to 40% of the respiratory signal’s dynamic range.

To facilitate qualitative and quantitative comparison with the original 4D MUSIC in this validation study, the CS-PI 4D MUSIC had the same number of cardiac phases as the original 4D MUSIC, but approximately half of the total acquisition time. Scanning parameters were: TR/TE= 2.9/0.9ms; flip angle, 25°; 0.6–0.9 mm true isotropic resolution without interpolation; FOV, 500*300*150 mm; 6–9 cardiac phases depending on heart rate; GRAPPA 2X-3X and 75% partial Fourier in both the phase encoding and partition encoding directions for the original 4D MUSIC, and 7X prospective variable density Poisson-Disk under-sampling for the CS-PI 4D MUSIC. Images from the original 4D MUSIC acquisition were reconstructed immediately with the vendor-provided image reconstruction pipeline, while data from the CS-PI 4D MUSIC acquisition were reconstructed on an external computer in less than 5 minutes using our custom image reconstruction framework shown in Fig. 2. During the 5 minutes where CS-PI 4D MUSIC images were being reconstructed offline, conventional multi-slice, multi-planar 2D cardiac cine images (20–25 cardiac phases, temporal resolution: 20–40ms) were acquired per our clinical protocol with VCBH using a spoiled gradient echo sequence.

Quantitative Measurements and Subjective Score

For our phantom study, both normalized root mean square errors (nRMSE) and structural similarity index (SSIM) (27) were calculated between each slice of the reference images and images reconstructed from the under-sampled data. The calculated nRMSE and SSIM were

averaged across all slices. Whereas reduction in nRMSE indicates greater fidelity to the original image, perfect identicality is represented by a SSIM value of 1 and the SSIM value decreases as the images differ.

For our in-vivo study, subjective image quality scores of 13 different anatomical region of interests (ROIs) were assessed: left/right atria, left/right ventricles, interatrial septum, interventricular septum, tricuspid valve, mitral valve, left/right ventricular outflow tracts, pulmonary arteries, ascending aorta and coronary arteries. Anonymized and randomized first-pass VCBH CE-MRA images, original 4D MUSIC images, and the CS-PI 4D MUSIC images were graded by two experienced cardiovascular MRI readers with greater than 2 years of experience in clinical cardiovascular MRI interpretation using a 4-point scale as outlined in Table 1. Evaluators were blinded to patient information and imaging techniques. Scores were independently provided by the two readers.

Vessel sharpness was quantitatively measured in the left ventricle and ascending aorta of the conventional first-pass CE-MRA, the original 4D MUSIC, and the CS-PI 4D MUSIC images by drawing a linear signal profile, as previously described (4). Specifically, sharpness is defined as the inverse of the distance (in mm) between the two points at 20% and 80% of the dynamic range. The end-systolic (ESV), end-diastolic (EDV) left ventricular volumes and ejection fractions (EF) based on the contrast-enhanced 2D cine short-axis images, the original 4D MUSIC and the CS-PI 4D MUSIC images were measured using a commercially available software (QMass, Medis, Netherlands). Note that these three sets of images were all acquired at end-expiration.

Statistical Analysis

All statistical analyses were conducted using the R software (28) and Excel (Microsoft, Redmond, WA). The three techniques (CE-MRA, MUSIC and CS-PI MUSIC) were compared using visual subjective image quality scores (ranging 1–4) in 13 ROIs and quantitative image sharpness in 2 ROIs. The weighted kappa coefficient was used to evaluate the inter-observer agreement for the subjective image quality score. The EDV, ESV and EF measurements were compared using Lin's concordance correlation coefficient and Bland-Altman analysis (29). Subjective quality scores from the average of two readers were compared in two steps per ROI: First, a Kruskal-Wallis test was used to compare among all three techniques; Second, if there was significant difference among the three techniques, post-hoc Dunn's tests would be performed to compare each of the three pairs of techniques (MUSIC vs. CS-PI MUSIC, CE-MRA vs. MUSIC, CE-MRA vs. CS-PI MUSIC). Both tests were performed for each of the 13 ROIs using a Bonferroni correction ($P<0.05/13=0.0038$). Similarly, quantitative image sharpness were compared in two steps after satisfying normality assumption: First, a one-way ANOVA test was used to test the differences among all three techniques; Second, if significant difference was found among the techniques, a post-hoc Tukey's honest significant difference (HSD) test would be performed for each of the three pairs of techniques. Both one-way ANOVA test and Tukey's HSD test were performed separately for the two ROIs (left ventricle and the ascending aorta) using a Bonferroni correction ($P<0.05/2=0.025$).

Results

Phantom Study

Table 2 shows comparative results of the SSIM and nRMSE between the regularly under-sampled data reconstructed using GRAPPA and the prospective randomly under-sampled data of similar acceleration factors reconstructed using ℓ_1 -ESPIRiT (19). The use of PI and CS together reduced the error between the fully-sampled reference and the under-sampled data. Figure 3 shows a slice of the reconstructed images using GRAPPA and ℓ_1 -ESPIRiT (19) at different acceleration factors. Substantial aliasing artifact is shown in the GRAPPA reconstructed images; ℓ_1 -ESPIRiT (19) offered reduced reconstruction error, even at higher acceleration factors.

In-vivo Study

All image acquisitions were successfully performed, with the scan time ranging from 7 to 10 minutes (8.9±1.2 min) for the original 4D MUSIC, and 4 to 6 minutes (4.6±0.4 min) for the CS-PI 4D MUSIC. Contrast-enhanced 2D multi-slice cardiac cine images were not acquired in 5 patients due to cardiopulmonary instability and concerns about possible blood oxygen desaturation during repeated VCBH.

Figure 4 shows a comparison of four images (first-pass, delayed-phase VCBH CE-MRA, the original 4D MUSIC and CS-PI 4D MUSIC) from a 12-month-old male patient. Intra-cardiac structures such as the cardiac chambers, trabeculae, and the aortic root were blurred by cardiac motion due to the lack of cardiac gating in first-pass and delayed-phase CE-MRA. These structures and other fine structures such as the aortic valve leaflets (dashed black arrow) were well delineated by both the original 4D MUSIC and the CS-PI 4D MUSIC. Note that the acquisition time for CS-PI 4D MUSIC was half of the original 4D MUSIC acquisition. The original 4D MUSIC and the CS-PI 4D MUSIC acquisitions enabled clear delineation of the left anterior descending coronary artery (Figure 4, bottom row), which was not possible with conventional first-pass CE-MRA.

The isotropic spatial resolution of both original 4D MUSIC and CS-PI 4D MUSIC allowed reformatting of acquired images into arbitrary 2D cine plane orientations, such as the four-chamber views and short-axis views (Figure 5). Comparing with conventional 2D cine images, both original 4D MUSIC and CS-PI 4D MUSIC images provided uniform blood-myocardium contrast, which is important for accurate and robust cardiac chamber segmentation and ventricular volume quantification.

Statistical Comparisons of Three Techniques

Two evaluators had moderate to excellent agreement for subjective image quality score, depending on the anatomical site (κ, range 0.46–0.96, Table 3). The average image quality scores were used in testing. In right atrium, for example, means (±SE) of the averaged quality image score were 1.8 (±0.2) for the first-pass CE-MRA, 3.9 (±0.2) for 4D MUSIC, and 3.9 (±0.2) for CS-PI MUSIC. The average image quality score provided by the two readers was significantly different among three techniques in all 13 regions of interest (all $P \leq 0.000042$). The subjective image quality scores of both the original 4D MUSIC and the

CS-PI 4D MUSIC were significantly higher than first-pass CE-MRA in all 13 regions of interest ($P \leq 0.0014$ for all comparisons). No significant difference was detected between the CS-PI 4D MUSIC and the original 4D MUSIC ($P \geq 0.42$ for all comparisons) despite the much shorter image acquisition time of the CS-PI 4D MUSIC sequence.

In the quantitative image sharpness, means (±SE) of first-pass CE-MRA, original 4D MUSIC and CS-PI 4D MUSIC were 0.36 (±0.08), 0.56 (±0.17), and 0.54 (±0.17) in ascending aorta and 0.22 (±0.07), 0.38 (±0.11), and 0.35 (±0.11) in the left ventricle, respectively. Image sharpness was significantly different among three techniques in both ascending aorta and left ventricle ($P= 0.021$ and $P=0.003$, respectively). Furthermore, both original 4D MUSIC and CS-PI 4D MUSIC showed significantly improved image sharpness than conventional first-pass CE-MRA at the ascending aorta and the LV chamber ($P \leq 0.023$ for all comparisons, Table 4). No significant difference was found between the original 4D MUSIC and the CS-PI 4D MUSIC at both the ascending aorta as well as the LV chamber ($P \geq 0.68$ for all comparisons).

Figure 6 shows the LV volume measurements and ejection fractions calculated based on conventional contrast-enhanced 2D cardiac cine, the original 4D MUSIC and CS-PI 4D MUSIC on 8 patients in whom short-axis 2D cine images were acquired. 4D MUSIC and CS-PI 4D MUSIC-derived volume measurements and ejection fractions correlated well with 2D cine MRI-derived measurements (all $r>0.90$ ad $r>0.85$, respectively).

Discussion

In this study, we demonstrated the feasibility of halving the acquisition time for high spatial resolution 4D (3D cine) ferumoxytol-enhanced MRI, without compromising image quality. Using a prospective random k-space under-sampling scheme, our CS-PI combined reconstruction method allowed for the acquisition of complete 4D datasets in less than 5 minutes, with a similar image reconstruction time. This technique offers the potential to replace the original 4D MUSIC and may be used to provide temporal resolution that is closer to standard 2D cine MRI.

With CS-PI 4D MUSIC, we were able to achieve similar, or sometimes better, image quality compared with the original 4D MUSIC due to several reasons. First, image artifacts caused by random under-sampling were incoherent rather than structured. This enabled higher acceleration factors without the structural artifacts that were sometimes observed in the original 4D MUSIC at higher acceleration factors. With a properly chosen regularization parameter λ that reflects the type of data acquired (MRA in our case) and number of iterations, the incoherent artifact induced by random under-sampling is gradually reduced as the iterative reconstruction proceeds. Second, due to the 50% reduction of acquisition time, drifts in the respiratory waveform as the effects of muscle relaxant wear off are less likely to occur. Third, the higher SNR provided by ferumoxytol allowed for more accurate coil sensitivity estimation (19) and effective noise removal with soft-thresholding (11), both of which support high acceleration factors while maintaining image quality.

Our custom-built, on-line image reconstruction system also improves the practicality of the proposed CS-PI 4D MUSIC technique in a clinical environment. The in-house system provided a platform for performing computationally intensive PI and CS combined image reconstruction algorithms outside vendor provided pipelines. At the same time, the default pipeline that includes vendor provided filters enabled reconstructed images to be sent back to the console with DICOM header information intact. Vendor provided k-space filters and image space correction ensured an accurate and unbiased comparison between original and CS-PI 4D MUSIC images, since some of the image correction algorithms, if not performed properly, may result in noticeable distortion of anatomy. Compared with (30), our iterative reconstruction was performed on an external computer instead of on the scanner. With our setup, reconstructions of subsequent clinical acquisitions are not delayed, and images reconstructed from iterative methods are provided inline and in a clinically acceptable timeframe (<5 minutes).

Balanced steady-state free precession (bSSFP) is the standard technique for 2D cardiac imaging at 1.5T due to excellent blood-myocardium contrast (31). Several attempts have been made to extend its utilization for 3D (32) or 4D (33) cardiac imaging. However, relative low SNR due to diminished in-flow enhancement in non-contrast bSSFP 3D/4D acquisitions limits achievable spatial resolution (e.g nominal resolution: $1.5\times1.5\times3.5$ mm^3 in (32)) or prolongs acquisition time (e.g nominal acquisition time: 14 minutes in (33)). In contrast, the proposed CS-PI 4D MUSIC technique can generate 0.6–0.9mm isotropic, non-interpolated resolution in a 4–5 minute acquisition by taking advantage of the higher available signal at 3.0T and strong R1 relaxivity of ferumoxytol.

In our CS-PI MUSIC data set, only 6–9 cardiac phases are reconstructed. For a typical heart rate of 120 bpm in our patient cohort, this corresponds to a temporal resolution of 50–80ms. Although such a temporal resolution might not be sufficient for accurate assessment for myocardial wall motion abnormalities, it appears to be sufficient for cardiac chamber volume measurements. As chamber volume quantification typically has higher priority than assessment of wall motion abnormality for our pediatric CHD patient population, we did not prolong our scan time in this study to achieve more cardiac phases. In this regard, incorporating k-t constraints in our image reconstruction could further accelerate our scanning and enable more cardiac phases without prolonging the scan time.

Ferumoxytol is an FDA approved intravenous iron supplement for iron deficiency anemia in patients with chronic kidney disease and has been used off-label as an MRI contrast agent in both adult (5, 24–26) and pediatric patients (4, 34–37). In March 2015, the FDA issued a boxed warning highlighting potential hypersensitivity reactions to ferumoxytol, which now requires a slow infusion rather than a bolus injection. Although some other iron oxide formulations are historically associated with risks including anaphylaxis/hypersensitivity reactions, ferumoxytol appears to be safer than other formulations (38). In a recent study of 8666 chronic kidney disease patients who underwent ferumoxytol administration, two patients (0.02%) experienced anaphylactoid reactions. There are little data in the literature regarding the safety profile of using ferumoxytol as an MRI contrast agent in pediatric patients. In our cohort of 13 pediatric CHD patients, no major or minor adverse reactions were noted. Experience in a larger cohort of patients is clearly needed to establish the safety

profile of ferumoxytol in the pediatric population. In our study, personnel and procedures were in place to deal with allergic reaction or other adverse events.

The high R1 relaxivity and long intra-vascular half-life of Ferumoxytol provide strong and stable enhancement of blood pool signal. However, ferumoxytol also has a stronger R2 relaxivity than conventional GBCA. To minimize the potential signal loss due to T2 relaxation, we used strong partial-echo readout (56%) to minimize TE (0.9ms in our protocol). In addition, to maximize the image contrast, which is determined by both T1 and T2 shortening effect, we carefully chose the contrast dose of 4mg/kg and flip angle of 25°, which provided satisfactory images for both CE-MRA and 4D MUSIC in our study. Further contrast dose and flip angle optimization may further improve the SNR of our acquisitions.

Although patients in our study were under anesthesia or sedation at time of imaging due to clinical need, the CS-PI 4D MUSIC can potentially be applied to patients during free-breathing using other forms of respiratory motion compensation strategies other than ventilator gating, such as diaphragmatic navigators or MR self-gating (39,40) techniques. Although the prospective under-sampling technique was evaluated in the context of evaluating cardiovascular anatomy, this technique may also be applicable to additional spatial/temporal resolution limited applications which may benefit from acquisition of multiple complete 3D volumes within an acceptable acquisition time.

Acknowledgments

Grant Support: NIH (NHLBI) R01HL127153

Abbreviations used

PI	parallel imaging
CS	compressed sensing
MUSIC	multiphase, steady-state imaging with contrast enhancement
GPU	graphics processing unit
CE-MRA	contrast-enhanced magnetic resonance angiography
GBCA	gadolinium-based contrast agent
USPIO	ultrasmall superparamagnetic iron-oxide
CMR	cardiac magnetic resonance
SENSE	sensitivity encoding
GRAPPA	generalized auto-calibrating partially parallel acquisitions
SNR	signal-to-noise ratio
GRE	gradient recalled echo

FFT	fast Fourier transform
CHD	congenital heart disease
NICU	neonatal intensive care unit
VCBH	ventilator-controlled breath-holding
TR	repetition time
TE	echo time
FOV	field of view
nRMSE	normalized root mean square errors
SSIM	structural similarity index
region of interest	ROI
LV	left ventricle
ESV	end-systolic volume
EDV	end-diastolic volume
EF	ejection fraction

References

1. Prince MR, Yucel EK, Kaufman JA, Harrison DC, Geller SC. Dynamic gadolinium-enhanced three-dimensional abdominal MR arteriography. J Magn Reson Imaging. 1993; 3:877–881. [PubMed: 8280977]
2. Saleh RS, Patel S, Lee MH, Boechat MI, Ratib O, Saraiva CR, Finn JP. Contrast-enhanced MR angiography of the chest and abdomen with use of controlled apnea in children. Radiology. 2007; 243:837–846. [PubMed: 17517937]
3. Prince MR, Narasimham DL, Stanley JC, Chenevert TL, Williams DM, Marx MV, Cho KJ. Breath-hold gadolinium-enhanced MR angiography of the abdominal aorta and its major branches. Radiology. 1995; 197:785–792. [PubMed: 7480757]
4. Han F, Rapacchi S, Khan S, Ayad I, Salusky I, Gabriel S, Plotnik A, Paul Finn J, Hu P. Four-dimensional, multiphase, steady-state imaging with contrast enhancement (MUSIC) in the heart: A feasibility study in children. Magn Reson Med. 2014; doi: 10.1002/mrm.25491
5. Li W, Tutton S, Vu AT, Pierchala L, Li BSY, Lewis JM, Prasad PV, Edelman RR. First-pass contrast-enhanced magnetic resonance angiography in humans using ferumoxytol, a novel ultrasmall superparamagnetic iron oxide (USPIO)-based blood pool agent. J Magn Reson Imaging. 2005; 21:46–52. [PubMed: 15611942]
6. Pruessmann KP, Weiger M, Scheidegger MB, Boesiger P. SENSE: sensitivity encoding for fast MRI. Magn Reson Med. 1999; 42:952–962. [PubMed: 10542355]
7. Griswold MA, Jakob PM, Heidemann RM, Nittka M, Jellus V, Wang J, Kiefer B, Haase A. Generalized autocalibrating partially parallel acquisitions (GRAPPA). Magn Reson Med. 2002; 47:1202–1210. [PubMed: 12111967]
8. Candes E, Romberg JT. Robust uncertainty principles: exact signal reconstruction from highly incomplete frequency information. IEEE Trans Inf Theory. 2006; 52:489–509.
9. Donoho D. Compressed sensing. IEEE Trans Inf Theory. 2006; 52:1289–1306.1.

10. Lustig M, Donoho D, Pauly JM. Sparse MRI: the application of compressed sensing for rapid MR imaging. Magn Reson Med. 2007; 58:1182–1195. [PubMed: 17969013]
11. Gamper U, Boesiger P, Kozerke S. Compressed sensing in dynamic MRI. Magn Reson Med. 2008; 59:365–373. [PubMed: 18228595]
12. Block KT, Uecker M, Frahm J. Undersampled radial MRI with multiple channels: iterative image reconstruction using a total variation constraint. Magn Reson Med. 2007; 57:1086–1098. [PubMed: 17534903]
13. Rudin L, Osher S, Fatemi E. Non-linear total variation noise removal algorithm. Phys D. 1992; 60:259–268.
14. Rapacchi S, Han F, Natsuaki Y, Kroeker R, Plotnik A, Lehman E, Sayre J, Laub G, Finn JP, Hu P. High spatial and temporal resolution dynamic contrast-enhanced magnetic resonance angiography using compressed sensing with magnitude image subtraction. Magn Reson Med. 2014; 71:1771–1783. [PubMed: 23801456]
15. Murphy M, Alley M, Demmel J, Keutzer K, Vasanawala S, Lustig M. Fast l_1 -SPIRiT compressed sensing parallel imaging MRI: scalable parallel implementation and clinically feasible runtime. IEEE Trans Med Imaging. 2012; 31:1250–1262. [PubMed: 22345529]
16. Wu, XL., Gai, J., Lam, F., Fu, M., Haldar, JP., Zhuo, Y., Liang, ZP., Hwu, WM., Sutton, BP. IMPATIENT MRI: Illinois massively parallel acceleration toolkit for image reconstruction with enhanced throughput in MRI. Proceedings of the 19th Annual Meeting of ISMRM; Montreal, Canada. 2011; Abstract 4396
17. Cook RL. Stochastic sampling in computer graphics. ACM Trans Graph. 1986; 5:51–72.
18. Wilman AH, Riederer SJ. Performance of an Elliptical Centric View Order for Signal Enhancement and Motion Artifact Suppression in Breath-hold Three-dimensional Gradient Echo Imaging. Magn Reson Med. 1997; 38:793–802. [PubMed: 9358454]
19. Uecker M, Lai P, Murphy MJ, Virtue P, Elad M, Pauly JM, Vasanawala SS, Lustig M. ESPIRiT-an eigenvalue approach to autocalibrating parallel MRI: where SENSE meets GRAPPA. Magn Reson Med. 2014; 71:990–1001. [PubMed: 23649942]
20. Uecker, M., Virtue, P., Ong, F., Murphy, MJ., Alley, MT., Vasanawala, SS., Lustig, M. Software toolbox and programming library for compressed sensing and parallel imaging. Proceedings of the ISMRM Workshop on Data Sampling and Reconstruction; Sedona, Arizona, USA. 2013;
21. BART: version 0.2.04. 2014.
22. Han, F., Zhou, Z., Sung, K., Paul Finn, J., Hu, P. A low-cost flexible non-linear parallelized MR image reconstruction system. Proc Intl Soc Mag Reson Med; Annual Meeting ISMRM; Toronto. 2015; 2015. p. 1535
23. Dagum L, Open MP. An industry standard API for shared-memory programming. IEEE Comput Sci Eng. 1998; 5:46–55.
24. Prince MR, Zhang HL, Chabra SG, Jacobs P, Wang Y. A pilot investigation of new superparamagnetic iron oxide (ferumoxytol) as a contrast agent for cardiovascular MRI. J Xray Sci Technol. 2003; 11:231–240. [PubMed: 22388293]
25. Sigovan M, Gasper W, Alley HF, Owens CD, Saloner D. USPIOenhanced MR angiography of arteriovenous fistulas in patients with renal failure. Radiology. 2012; 265:584–590. [PubMed: 22875796]
26. Bashir MR, Mody R, Neville A, Javan R, Seaman D, Kim CY, Gupta RT, Jaffe TA. Retrospective assessment of the utility of an iron-based agent for contrast-enhanced magnetic resonance venography in patients with endstage renal diseases. J Magn Reson Imaging. 2014; 40:113–118. [PubMed: 24130008]
27. Wang Z, Bovik AC, Sheikh HR, Simoncelli EP. Image quality assessment: from error visibility to structural similarity. IEEE Trans Image Process. 2004; 13:600–612. [PubMed: 15376593]
28. R Core Team. R: A language and environment for statistical computing. R Foundation for Statistical Computing; Vienna, Austria: 2013. http://www.R-project.org/
29. Lin LI. A concordance correlation coefficient to evaluate reproducibility. Biometrics. 1989; 45:255–268. [PubMed: 2720055]

30. Stalder AF, Schmidt M, Quick HH, Schlamann M, Maderwald S, Schmitt P, Wang Q, Nadar MS, Zenge MO. Highly undersampled contrast-enhanced MRA with iterative reconstruction: Integration in a clinical setting. Magn Reson Med. 2014; doi: 10.1002/mrm.25565

31. Carr JC, Simonetti O, Bundy J, Li D, Pereles S, Finn JP. Cine MR angi-ography of the heart with segmented true fast imaging with steady-state precession. Radiology. 2001; 219:828–834. [PubMed: 11376278]

32. Jung BA, Hennig J, Scheffler K. Single-breathhold 3D-trueFISP cinecardiac imaging. Magn Reson Med. 2002; 48:921–925. [PubMed: 12418009]

33. Li, F., Coppo, S., Piccini, D., Lim, RP., Stuber, M., Sodickson, DK., Otazo, R. Five-Dimensional Cardiac and Respiratory Motion-Resolved Whole-Heart MRI. Proc Intl Soc Mag Reson Med; Annual Meeting ISMRM; Toronto. 2015; 2015. p. 27

34. Thompson EM, Guillaume DJ, Dosa E, Li X, Nazemi KJ, Gahramanov S, Hamilton BE, Neuwelt EA. Dual contrast per-fusion MRI in a single imaging session for assessment of pediat-ric brain tumors. J Neurooncol. 2012; 109:105–114. [PubMed: 22528798]

35. Klenk C, Gawande R, Uslu L, Khurana A, Qiu D, Quon A, Doing J, Rosenberg J, Fineman SL, Moseley M, Link MED. Ionising radiation-free whole-body MRI versus 18F-fluorodeoxyglucose PET/CT scans for children and young adults with cancer: a prospective, non-randomised, single-centre study. Lancet Oncol. 2014; 15:275–285. [PubMed: 24559803]

36. Ruangwattanapaisarn N, Hsiao A, Vasanawala SS. Ferumoxytol as an off-label contrast agent in body 3T MR angiography: a pilot study in children. Pediatric Radiology. 2014; doi: 10.1007/s00247-014-3226-3

37. Nayak AB, Luhar A, Hanudel M, Gales B, Hall TR, Finn JP, Salusky IB, Zaritsky J. High-resolution, whole-body vascular imaging with ferumoxytol as an alternative to gadolinium agents in a pediatric chronic kidney disease cohort. Pediatric Nephrology. 2015; 30:515–521. [PubMed: 25212105]

38. Schiller B, Bhat P, Sharma A. Safety and effectiveness of ferumoxytolin hemodialysis patients at 3 dialysis chains in the United Statesover a 12-month period. Clin Ther. 2014; 36:70–83. [PubMed: 24315802]

39. Larson A, White R, Laub G, McVeigh E, Li D, Simonetti O. Self-gated cardiac cine MRI. Magn Res Med. 2004; 51:93–102.

40. Hu P, Hong S, Moghari MH, Goddu B, Goepfert L, Kissinger KV, Hauser TH, Manning WJ, Nezafat R. Motion correction using coil arrays (MOCCA) for free-breathing cardiac cine MRI. Magn Reson Med. 2011; 66:467–475. [PubMed: 21773986]

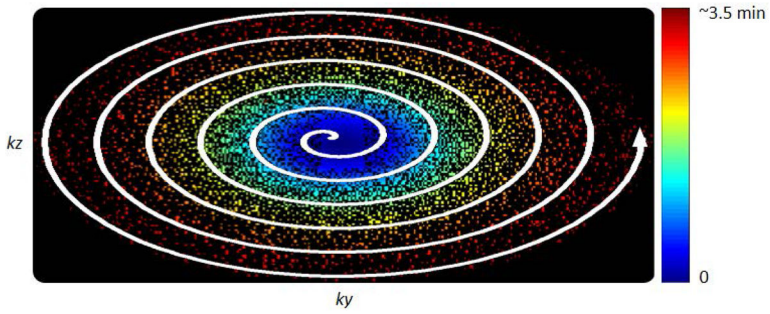

Figure 1.

Acquisition trajectory in k-space. A variable density Poisson-Disk k-space under-sampling pattern is used to accelerate MUSIC. The fully-sampled center and under-sampled outer k-space result in net acceleration factor of 7X. The trajectory for a single cardiac phase is depicted with samples colored according to their time of sampling from the start time of the acquisition. A center-out spiral arrow is added to reflect sampling order.

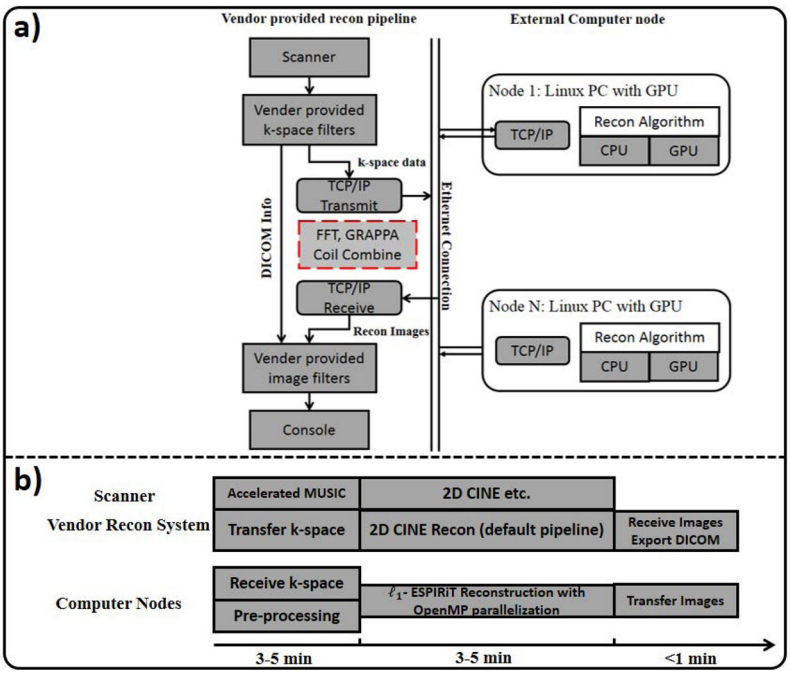

Figure 2.

a) Custom-built image reconstruction framework where one or more external computer nodes can be connected to the default vendor-provided reconstruction pipeline via TCP/IP. In current implementation, only one external Linux-based computer is connected to pipeline. b) Timeline of the CS-PI 4D MUSIC reconstruction process. K-space data are sent out to the external computer nodes once it is acquired during the scan. Immediately after center k-space region is acquired, pre-processing including coil compression coefficient matrix calculation and coil sensitivity maps estimation starts. Both are calculated in parallel with data receiving on external computer, and are usually done before the finish of data acquisition. It takes 3–5 minutes to reconstruct one 4D dataset (matrix size: 500*300*120*8) and additional 1 minute to send back the images. During the 3–5 minutes when the external computer processes the data, additional scans such as 2D CINE, 2D phase-contrast flow imaging may be acquired in parallel because the ℓ_1 -EPSIRiT reconstruction does not use any resources of the vendor provided reconstruction system.

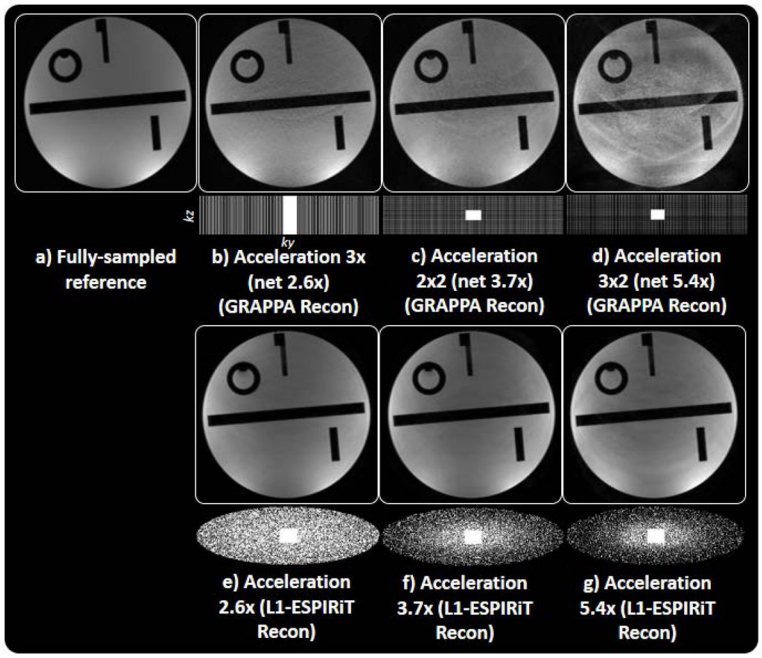

Figure 3.

Selected slice of reconstructed images from fully-sampled (a), regular under-sampled (b–d) and prospective randomly under-sampled data (e–g) with different acceleration factors. *ky* - *kz* under-sampling patterns are shown at the bottom of each selected slice. It can be seen that coherent aliasing artifacts and noise amplification increase as acceleration factor increases with traditional GRAPPA reconstruction, while image quality maintains with the use of ℓ_1 - ESPIRiT reconstruction on prospective randomly under-sampled data.

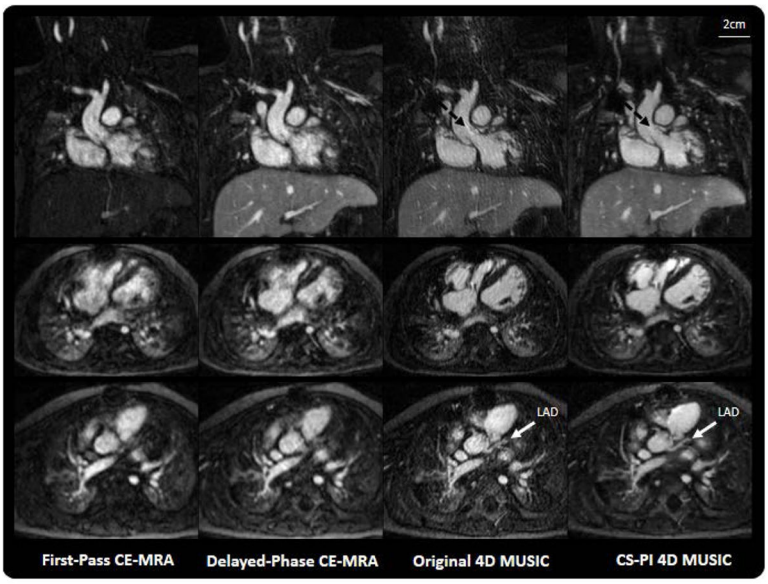

Figure 4.

First-pass, delayed-phase CE-MRA under VCBH (first and second column) versus original 4D MUSIC (third column) and the proposed CS-PI 4D MUSIC (fourth column) (phase #4 is chosen out of 7 cardiac phases for display) of a 12-month-old, 5.7kg boy. Acquisition times for the original 4D MUSIC and the CS-PI 4D MUSIC were 7 minutes and 3.75 minutes, respectively. CS-PI 4D MUSIC has less structural artifact compared to the original 4D MUSIC, despite its 50% reduced acquisition time. The artifact observed on original 4D MUSIC images is caused by high parallel imaging acceleration (GRAPPA 3X with 75% partial Fourier in ky,kz directions). The cardiac chambers, great vessels, as well as the aortic valve and the coronary arteries (white arrows) can be visualized in the original and CS-PI MUSIC acquisitions, but was poorly defined in the conventional first-pass and delayed-phase CE-MRA. The delayed-phase image was similar to the first-pass acquisition. The lack of structural artifacts in the CS-MUSIC image enable improved delineation of the aortic valve leaflets (black dashed arrows) compared to the original MUSIC.

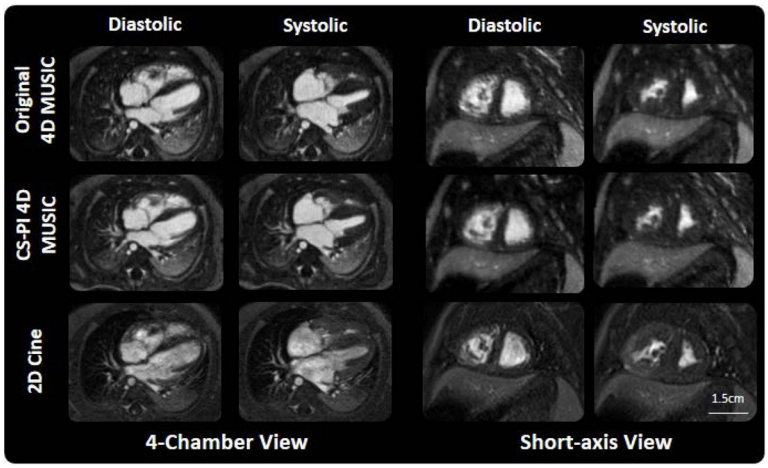

Figure 5.

Diastolic and systolic phase of reformatted cardiac four-chamber (left two columns) and short-axis (right two columns) views based on original 4D MUSIC (first row) and CS-PI 4D MUSIC (second row) in a 6-month-old, 3kg boy. The cardiac chambers were well delineated for both systole and diastole phases of the cardiac cycle using both the original 4D MUSIC and the CS-PI 4D MUSIC images, despite the shorter acquisition time of CS-MUSIC (4.8 min vs. 9 min). The 0.9 mm isotropic resolution in this patient enabled selection of arbitrary visualization plane without the loss of detailed structure.

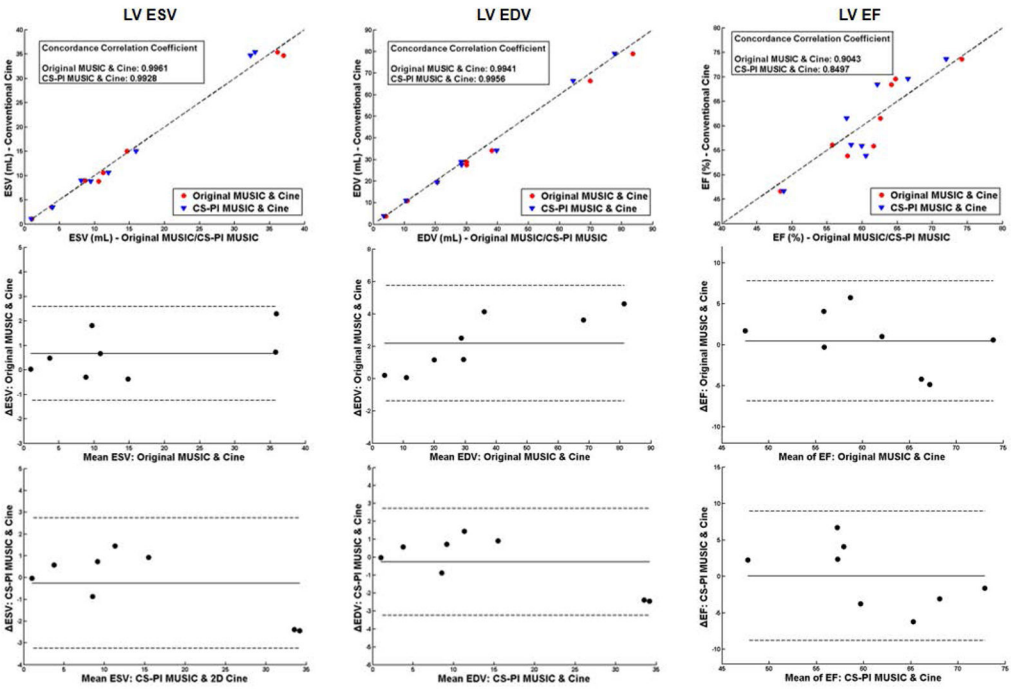

Figure 6.

Comparison of the left ventricle (LV) a): end-systolic volume (ESV), b): end-diastolic volume (EDV) and c): ejection fraction (EF) derived from conventional 2D cardiac cine, original 4D MUSIC and CS-PI 4D MUSIC on eight patients. Good correlation and agreement were found, as shown in the regression plot (top) and Bland-Altman analysis (middle and bottom).

Table 1

Image quality scoring criteria.

Atria and Ventricle	1: Not evaluable due to gross motion artifact and borders not defined 2: Non-uniform blood pool signal and wall motion artifact precludes confident evaluation of luminal contents 3: Uniform blood pool signal with mild wall motion artifact adequate for confident visualization of luminal contents 4: Uniform blood pool signal with no motion artifact such that the ventricular walls, septum, papillary muscles and trabeculae are sharply defined
Interatrial and Interventricular septum	1: Not visualized 2: Presence of septal tissue is seen 3: Probable septal continuity but small defects cannot be confidently excluded 4: Definite septal continuity and small defects can be confidently excluded
Tricuspid valve and Mitral valve	1: Not visualized due to gross motion artifact 2: Annulus visualized but borders poorly defined and cannot be confidently measured 3: Annulus clearly visualized and can be confidently measured but leaflets blurred 4: Annulus sharply defined and can be confidently measured and leaflets clearly visualized
LVOT, AV, and proximal aortic root RVOT, PV, and proximal MPA	1: Not evaluable due to gross motion artifact and borders not defined. 2: Outflow tract and annulus visualized but borders poorly defined and cannot be confidently measured 3: Outflow tract and annulus sharply defined and can be confidently measured but leaflets blurred 4: Outflow tract and annulus sharply defined and can be confidently measured and leaflets clearly visualized
Ascending aorta and Pulmonary artery	1: Not evaluable due to gross motion artifact with non-uniform luminal signal 2: Uniform luminal signal with poor definition of the wall due to motion 3: Uniform luminal signal with mild blurring of the wall due to motion 4: Uniform luminal signal with no motion blurring and sharply defined wall
Coronaries	1: Not evaluable due to gross motion artifact with visualization 2: Only origin of RCA and left main coronary can be identified 3: Origin and proximal course of RCA and LAD can be confidently visualized 4: Origin, proximal, and mid course of the RCA and LAD and proximal takeoff of LCx can be confidently visualized

AV aortic valve; **LAD** left anterior descending artery; **LCx** left circumflex artery; **LVOT** left ventricular outflow tract; **MPA** main pulmonary artery; **PV** pulmonic valve; **RCA** right coronary artery; **RVOT** right ventricular outflow tract

*Scores of 1 or 2 are considered non-diagnostic whereas scores of 3 or 4 are considered diagnostic

Table 2

Normalized root-mean square errors (nRMSE) and structural similarity index (SSIM) average values between fully-sampled reference image and images reconstructed from GRAPPA-accelerated/prospectively random under-sampled data. The background noise was excluded from measurement by using only pixels within the upper 90% intensity scale for both calculations.

	nRMSE	SSIM
GRAPPA 3x	0.045	0.877
GRAPPA 2x2	0.069	0.802
GRAPPA 3x2	0.098	0.737
L1-EPSIRiT 2.6x	0.029	0.982
L1-EPSIRiT 3.7x	0.035	0.945
L1-EPSIRiT 5.4x	0.048	0.902

Table 3

Subjective image quality scores provided by two readers and weighted kappa coefficients κ for different anatomic sites and imaging techniques.

Cardiovascular Structure	Reader 1/Reader 2 (Mean ± SE)			Average Score (Mean ± SE)			κ		
	4D MUSIC	*CS-PI MUSIC*	*First-pass CE-MRA*	*4D MUSIC*	*CS-PI MUSIC*	*First-pass CE-MRA*	*4D MUSIC*	*CS-PI MUSIC*	*First-pass CE-MRA*
Right Atrium	**3.8±0.4/4.0±0**	**3.8±0.4/4.0±0**	**1.9±0.3/1.8±0.4**	**3.9±0.2**$^{(*)}$	**3.9±0.2**$^{(*)}$	**1.8±0.2**	**0.87**	**0.87**	**0.88**
Left Atrium	**4.0±0/3.8±0.3**	**4.0±0/3.8±0.3**	**2.2±0.4/2.4±0.7**	**3.9±0.2**$^{(*)}$	**3.9±0.2**$^{(*)}$	**2.3±0.5**	**0.84**	**0.85**	**0.88**
Right Ventricle	**4.0±0/3.7±0.4**	**4.0±0/3.6±0.6**	**2.0±0/2±0.4**	**3.8±0.2**$^{(*)}$	**3.8±0.3**$^{(*)}$	**2±0.2**	**0.85**	**0.8**	**0.88**
Left Ventricle	**3.9±0.3/3.8±0.4**	**3.9±0.2/3.8±0.4**	**2.0±0/2.3±0.4**	**3.8±0.2**$^{(*)}$	**3.8±0.2**$^{(*)}$	**2.1±0.2**	**0.86**	**0.85**	**0.88**
Interatrial Septum	**3.8±0.5/3.8±0.4**	**3.9±0.3/3.8±0.4**	**2.1±0.9/2.2±0.7**	**3.8±0.4**$^{(*)}$	**3.9±0.2**$^{(*)}$	**2.1±0.7**	**0.96**	**0.84**	**0.88**
Interventricular Septum	**3.9±0.2/4.0±0**	**3.8±0.4/4.0±0**	**2.5±0.5/3.0±0.6**	**4±0.1**$^{(*)}$	**3.9±0.2**$^{(*)}$	**2.8±0.5**	**0.85**	**0.82**	**0.88**
Tricuspid Valve	**4.0±0/3.7±0.4**	**4.0±0/3.7±0.6**	**1.4±0.5/2.0±0**	**3.8±0.2**$^{(*)}$	**3.8±0.3**$^{(*)}$	**1.7±0.3**	**0.78**	**0.81**	**0.88**
Mitral Valve	**4.0±0/3.7±0.4**	**4.0±0/3.7±0.6**	**1.4±0.5/2.0±0**	**3.8±0.2**$^{(*)}$	**3.8±0.3**$^{(*)}$	**1.7±0.3**	**0.78**	**0.81**	**0.88**
LVOT	**3.9±0.2/3.3±0.6**	**3.9±0.3/3.5±0.5**	**3.0±0.2/2.3±0.6**	**3.7±0.3**$^{(*)}$	**3.7±0.2**$^{(*)}$	**2.5±0.2**	**0.48**	**0.53**	**0.88**
RVOT	**3.9±0.1/3.3±0.4**	**3.9±0.5/3.3±0.4**	**3.1±0.4/2.5±0.6**	**3.7±0.2**$^{(*)}$	**3.7±0.2**$^{(*)}$	**2.5±0.4**	**0.49**	**0.51**	**0.88**
Pulmonary Artery	**3.8±0.4/3.7±0.4**	**4.0±0/3.9±0.3**	**3.3±0.3/3.5±0.5**	**3.8±0.2**$^{(*)}$	**4±0.1**$^{(*)}$	**3.2±0.3**	**0.85**	**0.86**	**0.88**
Ascending Aorta	**3.9±0.3/3.8±0.3**	**4.0±0/3.9±0.3**	**3.1±0.3/3.7±0.5**	**3.9±0.2**$^{(*)}$	**4±0.1**$^{(*)}$	**3.3±0.3**	**0.86**	**0.85**	**0.88**
Coronary	**3.6±0.9/3.0±1.1**	**3.6±0.9/3.1±1.1**	**1.1±0.3/1.2±0.4**	**3.2±0.9**$^{(*)}$	**3.3±0.9**$^{(*)}$	**1.1±0.2**	**0.46**	**0.52**	**0.88**

$^{(*)}$denotes statistical significance (P<0.05/13=0.0038) when compared with ferumoxytol-based first-pass CE-MRA.

Table 4

Vessel sharpness (mm^{-1}) measured in the ascending aorta and left ventricle of the conventional first-pass CE-MRA, the original 4D MUSIC, and the CS-PI 4D MUSIC.

	Ascending Aortic (Mean ± SE)	**Left Ventricle Chamber (Mean ± SE)**
First-pass CE-MRA	0.36±0.08	0.22±0.07
Original 4D MUSIC	0.56±0.17*(*)*	0.38±0.11*(*)*
CS-PI 4D MUSIC	0.54±0.17*(*)*	0.35±0.11*(*)*

*(*)*denotes statistical significance (P<0.05/2=0.025) when compared with ferumoxytol-based first-pass CE-MRA.